Acta Crystallographica Section D
Biological Crystallography
ISSN 1399-0047

Structural insights into the mechanism of calmodulin binding to death receptors

Peng Cao,[a]‡ Wenting Zhang,[a,c]‡ Wenjun Gui,[a] Yuhui Dong,[b] Tao Jiang[a]* and Yong Gong[b]*

[a]National Laboratory of Biomacromolecules, Institute of Biophysics, Chinese Academy of Sciences, 15 Datun Road, Chaoyang District, Beijing 100101, People's Republic of China, [b]Beijing Synchrotron Radiation Facility, Institute of High Energy Physics, Chinese Academy of Sciences, 19B Yuquan Road, Shijingshan District, Beijing 100049, People's Republic of China, and [c]University of Chinese Academy of Sciences, 19A Yuquan Road, Beijing 100049, People's Republic of China

‡ These authors contibuted equally to this work.

Correspondence e-mail: tjiang@sun5.ibp.ac.cn, yonggong@ihep.ac.cn

Received 23 August 2013
Accepted 28 March 2014

PDB references: calmodulin, complex with p75^{NTR} helix 5, 3ewv; complex with Fas helix 1, 3ewt

The death receptors Fas, p75^{NTR} and DR6 are key components of extrinsically activated apoptosis. Characterization of how they interact with the adaptors is crucial in order to unravel the signalling mechanisms. However, the exact conformation that their intracellular death domain adopts upon binding downstream partners remains unclear. One model suggests that it adopts a typical compact fold, whilst a second model proposed an open conformation. Calmodulin (CaM), a major calcium sensor, has previously been reported to be one of the Fas adaptors that modulate apoptosis. This work reports that CaM also binds directly to the death domains of p75^{NTR} and DR6, indicating that it serves as a common modulator of the death receptors. Two crystal structures of CaM in complexes with the corresponding binding regions of Fas and p75^{NTR} are also reported. Interestingly, the precise CaM-binding sites were mapped to different regions: helix 1 in Fas and helix 5 in p75^{NTR} and DR6. A novel 1–11 motif for CaM binding was observed in p75^{NTR}. Modelling the complexes of CaM with full-length receptors reveals that the opening of the death domains would be essential in order to expose their binding sites for CaM. These results may facilitate understanding of the diverse functional repertoire of death receptors and CaM and provide further insights necessary for the design of potential therapeutic peptide agents.

1. Introduction

Apoptosis, a physiological and highly regulated mechanism for inducing cell death, is triggered by signalling through members of the tumour necrosis factor receptor (TNFR) superfamily, also known as death receptors in the extrinsic pathway. To date, eight death receptors have been identified in humans: Fas (CD95), TNFR1 (tumour necrosis factor receptor 1), p75^{NTR} (neurotrophin receptor), DR3, DR4 (TRAIL-R1), DR5 (TRAIL-R2), DR6 and EDAR (ectodysplasin A receptor) (Lavrik *et al.*, 2005). Abnormal expression or activity of these receptors can lead to diseases such as cancer, problems in the immune system and neurodegenerative diseases. Death receptors are characterized by the presence of a death domain, which is a conserved ∼80-residue motif within their cytoplasmic segments (Fig. 1*a*). This domain adopts a 'Greek-key' topology with six helices (termed helices 1–6; Mc Guire *et al.*, 2011; Park *et al.*, 2007; Wilson *et al.*, 2009). Some intracellular proteins, such as FADD (Fas-associated death domain protein), TRADD (tumour necrosis factor receptor type 1-associated death-domain protein) and RAIDD (RIP-associated ICH-1 homologous protein with a death domain), also contain death domains. Although lacking intrinsic catalytic activity, the death domains can trigger signal transduction pathways through binding adaptor proteins in the presence of

an appropriate stimulus. Interestingly, whilst all death domains share a similar architecture of six helices, they are highly specific in recruiting different primary adaptors. FADD is the primary binding partner for the death domains of Fas, DR4 and DR5. TRADD is the primary binding partner of TNF-R1, DR3 and DR6. In contrast, $p75^{NTR}$ functions either through cooperating with different co-receptors or by signalling independently through adaptors devoid of death domains (Gong *et al.*, 2008; Ibáñez & Simi, 2012).

Investigation of the structural basis of interactions between death domains and downstream adaptor proteins is crucial for understanding their physiological functions and ultimately for the design of powerful therapeutic agents. However, only a few contradictory crystal structures are available to date; therefore, it remains unclear what the exact structure during interaction might be. In 2009, a high-resolution structure of the Fas–FADD complex was published with an unexpected open mode of the Fas death domain, which was regarded as a base and switch for FADD binding and subsequent DISC (death-inducing signalling complex) formation (Scott *et al.*, 2009; Salvesen & Riedl, 2009). The open Fas death domain exhibits an elongated conformation, not a globular one in a compact huddle fold as previously suggested (Park *et al.*, 2007). A subsequent low-resolution structure of the Fas–FADD complex proposed the view that Fas and FADD form an oligomeric structure without opening, a result that was also in agreement with the traditional model (Wang *et al.*, 2010; Ferrao & Wu, 2012). These contradictory results suggest that distinct signalling conformations exist for Fas and other death receptors.

Calmodulin (CaM) is one of the adaptor proteins of Fas (Ahn *et al.*, 2004; Wu *et al.*, 2005). As the major intracellular Ca^{2+} sensor and effector protein, CaM is a key mediator and regulator of cellular signalling (Hoeflich & Ikura, 2002). A large number of structural and functionally diverse effectors are targets of CaM, an interaction that mediates a plethora of fundamental processes. CaM binds directly to the death domain of Fas in a Ca^{2+}-dependent manner, and functions in Fas-mediated cell apoptosis through regulation of DISC formation. Trifluoperazine, a CaM antagonist, has been reported to affect Fas-mediated DISC formation through modulating CaM binding to Fas (Chen *et al.*, 2008; Pan *et al.*, 2011). CaM has also been shown to be required for neuronal survival maintained by neurotrophins (Egea *et al.*, 2000, 2001). Ca^{2+} signalling has been found to play an important role in the development of the mammalian nervous system through regulating the motility and guidance of nerve growth cones triggered by guidance factors (Hong *et al.*, 2000; Li *et al.*, 2005). Coincidently, both $p75^{NTR}$ and DR6 are abundantly expressed by developing neurons during early nervous development in mammals (Benschop *et al.*, 2009; Ibáñez & Simi, 2012). In summary, these facts suggest an as yet unidentified cross-talk mechanism between the Ca^{2+} signal, CaM and the death receptors $p75^{NTR}$ and DR6.

Here, we found that both $p75^{NTR}$ and DR6 can directly interact with CaM in a Ca^{2+}-dependent manner in a similar fashion to Fas. Using X-ray diffraction, the high-resolution structures of CaM in complex with binding regions derived from either $p75^{NTR}$ or Fas have been solved. Furthermore, we present two models of complexes between the full-length receptors and CaM.

2. Materials and methods

2.1. Cells, antibodies and reagents

PC-12 cells were purchased from the Cell Culture Facility in the Institute of Basic Medical Sciences of the Chinese Academy of Medical Sciences. CaM-Sepharose 4B was purchased from Amersham Biosciences. The polyclonal antibodies were purchased from Santa Cruz Biotechnology (Santa Cruz, California, USA).

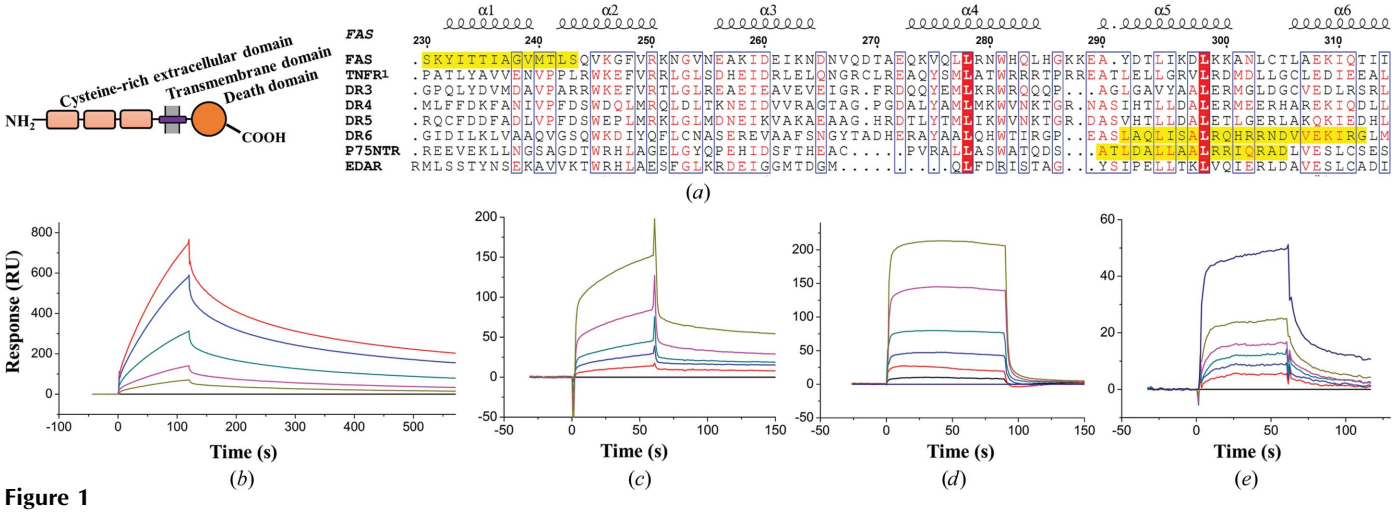

Figure 1
Binding of CaM to the death receptors. (*a*) Schematic representation of the common domains of human death receptors and sequence alignment of their death domains. The confirmed CaM-binding regions are highlighted in yellow. EDAR, ectodysplasin A receptor. (*b*) Real-time binding of CaM to $p75^{NTR}$ death domain analyzed by SPR assay. CaM at various concentrations (from top to bottom: 60, 40, 20, 10, 5 and 0 μM) were injected onto the chip surface covered by the death domain. (*c*)–(*e*) Real-time binding of the Fas (*c*), $p75^{NTR}$ (*d*) and DR6 (*e*) peptides to CaM.

2.2. Peptide synthesis and purification

All synthetic human peptides were synthesized by HD Biosciences Co. Ltd (Shanghai, People's Republic of China) with a purity above 98%. The peptides were purified by reversed-phase HPLC and analyzed by mass spectrometry to confirm their molecular weights.

2.3. Protein expression and purification

Recombinant human CaM with an N-terminal six-histidine tag was expressed using pET-28a vector and *Escherichia coli* strain BL21 (DE3) (Novagen). The protein was purified to homogeneity by affinity chromatography and gel filtration (Superdex 75, GE Healthcare) with the buffer 50 m*M* Tris–HCl pH 8.0, 150 m*M* NaCl, 2 m*M* $CaCl_2$. For the SPR assay, recombinant CaM was biotinylated with biotin-XX, SSE (Molecular Probes, Eugene, Oregon, USA) and was purified as described previously (Kincaid *et al.*, 1988).

Recombinant rat $p75^{NTR}$ death domain was expressed using *E. coli* strain BL21 (DE3) (Novagen) transformed with pET-24a vector containing the sequence for the $p75^{NTR}$ death domain and a C-terminal six-histidine tag sequence. The protein was purified by affinity chromatography and size-exclusion chromatography (Superdex 200, GE Healthcare) with the buffer 50 m*M* Tris–HCl pH 7.5, 150 m*M* NaCl.

For crystallization, CaM and the peptide were mixed in a molar ratio of 1:1.5 and the complex was further purified on a gel-filtration column prior to concentration to approximately 17 mg ml^{-1} in 2 m*M* $CaCl_2$.

2.4. CaM-Sepharose pull-down assay and Western blotting

PC-12 cells were lysed in lysis buffer (PBS buffer containing 1% Triton X-100 and proteinase inhibitor) with either 1 m*M* $CaCl_2$ or 1 m*M* EGTA and were then incubated with CaM-Sepharose 4B for 1 h at 4°C. After incubation, the beads were washed at least three times with PBS buffer containing 1% Triton X-100 in 1 m*M* $CaCl_2$ or 1 m*M* EGTA to remove nonspecifically bound proteins. After washing, the beads were boiled in the loading buffer and the proteins in the supernatant were separated by SDS–PAGE.

For Western blotting, proteins were transferred to a polyvinylidene difluoride membrane (Millipore Co.). After blocking with 5% nonfat milk, the membranes were incubated with primary antibody (200 μg ml^{-1}) followed by peroxidase-conjugated anti-rabbit IgG (1:2000 dilution). Blots were developed using enhanced chemiluminescence Western blotting detection reagents.

2.5. Surface plasmon resonance (SPR)

Real-time binding and kinetic analyses by SPR were carried out on a BIAcore3000 instrument at 25°C. The SPR signal was expressed in relative response units (RU), *i.e.* the response obtained in a control flow channel was subtracted from the SPR signal. The eluent consisted of 150 m*M* NaCl, 50 m*M* HEPES pH 7.4, 1 m*M* $CaCl_2$, 0.005% Tween-20.

In the analysis of the interaction of the death domain with CaM, the death domain was immobilized on a CM5 chip using an amine coupling kit, and the remaining coupling sites were blocked with 1 *M* ethanolamine pH 8.5. CaM at various concentrations was injected over the chip surface and a blank flow cell for 2 min at a flow rate of 30 μl min^{-1}. After each analytic cycle, the sensor chip was regenerated in 10 m*M* NaOH. The curves were fitted to a 1:1 Langmuir binding model (*BIAevaluation* 4.1 software) to obtain equilibrium dissociation constants.

In the qualitative analysis of CaM–peptide interaction, the SA chip was preconditioned with 1 *M* NaCl in 50 m*M* NaOH, and biotinylated CaM was immobilized over the streptavidin surface. Fas, $p75^{NTR}$ or DR6 peptides at various concentrations were injected over the CaM surface and a blank flow cell for 1 min at a flow rate of 30 μl min^{-1}.

2.6. Crystallization and structure determination

The complexes were crystallized by hanging-drop vapour diffusion at 20°C. The crystallization condition for the $p75^{NTR}$ complex was 27%(*w*/*v*) PEG 8000, 0.1 *M* magnesium acetate, 0.1 *M* ammonium acetate, 0.05 *M* sodium cacodylate pH 4.7 and that for the Fas complex was 25%(*w*/*v*) PEG 8000, 0.2 *M* sodium acetate, 0.1 *M* sodium cacodylate pH 5.5. Before data collection, the crystals were cryoprotected by soaking them in mother liquor containing 15%(*v*/*v*) glycerol and flash-cooled. X-ray diffraction data were collected using in-house Cu $K\alpha$ X-rays generated by a Rigaku MicroMax-007 rotating-anode X-ray source and a Rigaku R-AXIS IV^{++} imaging-plate area detector. The data were integrated and scaled with *DENZO* and *SCALEPACK* (Otwinowski & Minor, 1997).

Both structures were determined by molecular replacement using *MOLREP* (Vagin & Teplyakov, 2010) from the *CCP*4 program suite (Winn *et al.*, 2011). The protein portions of the CaM–trifluoperazine complex (PDB entry 1lin; Vandonselaar *et al.*, 1994) and the CaM–myristoylated CAP-23/NAP-22 peptide complex (PDB entry 1l7z; Matsubara *et al.*, 2004) were used as initial search models. Refinement was carried out with *CNS* (Brünger *et al.*, 1998) and *REFMAC* (Murshudov *et al.*, 2011). Model building was carried out using *Coot* (Emsley & Cowtan, 2004). The Ramachandran plots generated using *PROCHECK* (Laskowski *et al.*, 1993) showed that >90% of the residues were in the most favourable region and no residues were in the disallowed region. Details of data collection and structure refinement are presented in Table 1. The figures were prepared using *ESPript* (Gouet *et al.*, 1999), *PyMOL* (http://www.pymol.org) and *LIGPLOT* (Wallace *et al.*, 1995).

3. Results

3.1. Binding of CaM to the death receptors $p75^{NTR}$, DR6 and Fas

Direct interaction between CaM and the death receptors was demonstrated using a CaM pull-down assay in combination with surface plasmon resonance (SPR) measurements. In the pull-down assay, PC-12 cell lysates were incubated with

CaM-conjugated Sepharose and then Western-blotted with a receptor antibody. Because most CaM–target binding is Ca^{2+}-dependent, the lysis buffer was supplemented with 1 m*M* Ca^{2+}. Our results showed that $p75^{NTR}$ was detected in the CaM-Sepharose-bound proteins. The binding was abolished in the presence of 1 m*M* EGTA, indicating that $p75^{NTR}$ interacted with CaM in a Ca^{2+}-dependent manner (Supplementary Fig. S1*a*[1]). Similar results were obtained for DR6 binding studies. To measure the real-time interaction dynamics, we expressed the recombinant death domain of $p75^{NTR}$, immobilized it on a CM5 chip for SPR studies and evaluated the binding over a wide range of CaM concentrations (Fig. 1*b*). CaM bound the $p75^{NTR}$ death domain with a dissociation constant (K_d) of 3.29×10^{-5} *M*, indicating that interaction between these two proteins can occur in a direct manner. When active Ca^{2+} was removed from the running buffer, *i.e.* in the presence of 1 m*M* EGTA, no specific interaction was detected.

Next, we mapped the precise CaM-binding sites on Fas, $p75^{NTR}$ and DR6. Initially, all possible interacting peptides were synthesized according to their sequences. Subsequently, binding profiles were obtained through size-exclusion chromatography and gel mobility-shift and SPR assays. Firstly, the CaM–peptide complex eluted later than the unbound protein upon gel-filtration chromatography (Supplementary Figs. S1*b* and S1*c*). Secondly, the gel mobility-shift results showed different shifts for samples that were bound or unbound to the peptide in the presence of Ca^{2+} by native PAGE (Supplementary Fig. S1*d*). Thirdly, the interactions were demonstrated by SPR assay (Figs. 1*c*, 1*d* and 1*e*). Biotinylated CaM was immobilized onto the SA chip and the peptides were injected over the chip surface at different concentrations. The K_d values were calculated as 1.95×10^{-5}, 2.48×10^{-4} and 3.57×10^{-6} *M* for the Fas, $p75^{NTR}$ and DR6 peptides, respectively. From the above indicators and our structural data (discussed below), we confirmed that the CaM-binding regions are the first helix (helix 1) of the Fas death domain and the fifth helix (helix 5) of both the $p75^{NTR}$ and DR6 death domains (Fig. 1*a*).

3.2. Crystal structure of the $p75^{NTR}$–CaM complex

To clarify the structural basis of the observed interaction between $p75^{NTR}$ and CaM, we determined the crystal structure of CaM bound to $p75^{NTR}$ helix 5 (^{394}ATLDALLAALRR-IQRAD^{410}) at 2.6 Å resolution. The overall structure of the $p75^{NTR}$–CaM complex (Figs. 2*a* and 2*b*) shows that CaM engulfs the α-helix peptide with its two Ca^{2+}-binding lobes through extensive interactions. Density for all 17 residues was observed and unambiguously defined in the electron-density map (Fig. 2*c*). CaM forms a closed ellipsoidal conformation. Two lobes are folded in such a way that CaM can grab the target peptide in an antiparallel orientation in which the N-lobe mainly binds to the C-terminal portion of the peptide. The peptide and CaM bury a total area of about 2218 Å^2, of which roughly 60% is hydrophobic as calculated by *CNS* (Brünger *et al.*, 1998). The interactions of the N-lobe and C-lobe with helix 5 are not equivalent in the amount of buried surface area; the N-lobe buries a larger total surface than the C-lobe, suggesting that the N-lobe may bind the peptide more tightly. It is worth noting that Arg404 and Arg405 of helix 5, which are two critical basic residues that induce the pro-apoptotic effect of $p75^{NTR}$ (Rabizadeh *et al.*, 2000), are in contact with the CaM residues Met71, Met72 and Glu84 *via* hydrogen-bond interactions (Fig. 2*c*).

The crystal structure reveals two unusual structural features compared with other CaM–peptide complexes. The most striking feature is the CaM-binding motif, which is located between the two key hydrophobic anchors. The target peptides always anchor to CaM using two bulky hydrophobic anchor residues, which interact with the N-lobe and the C-lobe, respectively. There are diverse CaM-binding motifs which are grouped into different classes, such as 1–14, 1–10, 1–16 and 1–17, according to the spacing between the two anchors (Maximciuc *et al.*, 2006; Meador *et al.*, 1992, 1993; Osawa *et al.*, 1999). In our structure, the lobes of CaM contact two key anchors (Ile406 and Leu396) with a novel 1–11 spacing, which does not conform to any other known CaM-binding mode

Table 1
Data-collection and refinement statistics.

	CaM–$p75^{NTR}$	CaM–Fas
Data collection		
Wavelength (Å)	1.5418	1.5418
Space group	$P3_221$	$P3_221$
Unit-cell parameters		
$a = b$ (Å)	39.9	40.1
c (Å)	182.0	174.4
$\alpha = \beta$ (°)	90.0	90.0
γ (°)	120.0	120.0
Solvent content	0.46	0.45
Resolution (Å)	15–2.6 (2.66–2.60)	20–2.4 (2.46–2.40)
R_{merge}†	0.05 (0.10)	0.04 (0.13)
$\langle I/\sigma(I)\rangle$	37.2 (10.0)	40.7 (10.3)
Completeness (%)	99.0 (98.4)	99.6 (97.3)
Multiplicity	7.3 (5.5)	8.6 (6.8)
Refinement		
Resolution (Å)	15–2.6	20–2.4
No. of reflections	5369	6575
R_{work}/R_{free}‡	0.228/0.282	0.217/0.259
No. of atoms		
Protein	1121	1125
Peptide	131	102
Ion	4	4
Water	90	44
B factors (Å^2)		
Protein	25.7	35.7
Peptide	33.6	44.0
Ion	19.4	28.6
Water	30.5	31.9
R.m.s. deviations		
Bond lengths (Å)	0.014	0.011
Bond angles (°)	1.6	1.4
Ramachandran statistics, residues in (%)		
Most favoured regions	90.3	94.9
Allowed regions	9.7	5.1
Disallowed regions	0	0
PDB code	3ewv	3ewt

† $R_{merge} = \sum_{hkl}\sum_i |I_i(hkl) - \langle I(hkl)\rangle| / \sum_{hkl}\sum_i I_i(hkl)$, where *hkl* indicates unique reflection indices and *i* indicates symmetry-equivalent indices. ‡ $R_{work} = \sum_{hkl} ||F_{obs}| - |F_{calc}|| / \sum_{hkl} |F_{obs}|$, where $|F_{obs}|$ and $|F_{calc}|$ are the observed and calculated structure-factor amplitudes, respectively. R_{free} is calculated using 5% of the reflections that were randomly excluded from refinement.

[1] Supporting information has been deposited in the IUCr electronic archive (Reference: XB5078).

(Fig. 2*d*). The 1–11 spacing places the two anchors on opposite faces of the continuous helix. Superposition of the individual lobes with the complex between CaM and the peptide from smooth muscle myosin light-chain kinase (smMLCK; Meador *et al.*, 1992), which employs the 1–14 motif, shows that the anchors interact with local elements of CaM in similar ways (Supplementary Fig. S2). The anchor Ile406 is deeply buried in the CaM N-lobe hydrophobic pocket formed by Phe19, Leu32,

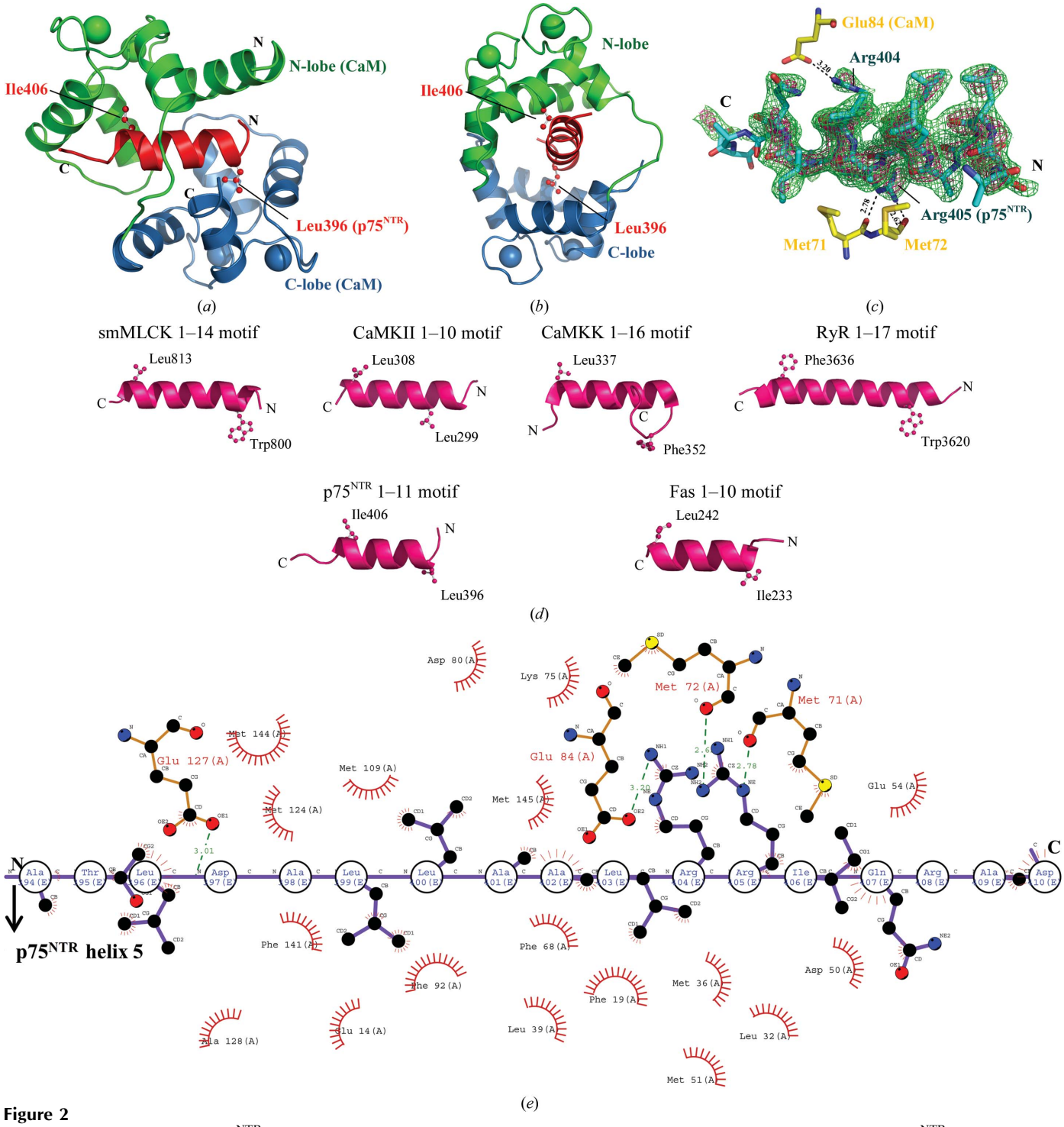

Figure 2
Crystal structure of the CaM–p75^{NTR} complex. (*a*) Ribbon diagram of the complex. Green, CaM N-lobe; blue, CaM C-lobe; red, p75^{NTR} helix 5. Two key anchors (Leu396 and Ile406) are shown in ball-and-stick representation. Ca^{2+} ions are represented as spheres. (*b*) 90° rotation of (*a*). (*c*) A $2F_o - F_c$ peptide-omitted electron-density map (green, contoured at 1σ) and a $F_o - F_c$ map (red, contoured at 3σ) for p75^{NTR} helix 5. Local interactions are shown between CaM residues (yellow sticks) and Arg404 and Arg405 of p75^{NTR} (blue sticks), both of which appear to be critical for p75^{NTR}-induced apoptosis as reported previously (Rabizadeh *et al.*, 2000). (*d*) Different motifs are shown for comparison with p75^{NTR} (1–11 motif) and Fas (1–10 motif). (*e*) *LIGPLOT* diagram detailing the interactions between CaM and p75^{NTR}. The red eyelash shapes mark the CaM residues that make hydrophobic contacts with p75^{NTR} helix 5. Hydrogen bonds are shown as dashed green lines.

Met36, Val55, Ile63, Phe68 and Met71. The other anchor Leu396 makes extensive contacts with the deep hydrophobic cavity in the CaM C-lobe formed by Phe92, Leu105, Met124, Ala128, Val136, Phe141 and Met144. Besides the two anchors, three bulky hydrophobic residues (Leu399, Leu400 and Leu403) and a set of alanines make extensive interactions with the CaM tunnel (Fig. 2*e*). Thus, the peptide is firmly anchored to CaM by multiple hydrophobic interactions.

The other unusual feature concerns the orientation of p75^{NTR} helix 5 with respect to the N-lobe and C-lobe of CaM. Previous work proposed that the distribution of positive charges on the peptides was an important determinant of the binding orientation to CaM (Vetter & Leclerc, 2003). A cluster of basic residues were often found on the peptides, which were bound to the more acidic residues of the CaM channel outlet, contributed mainly by the C-lobe. Based on this argument, a parallel oriented binding might have been predicted for p75^{NTR} because there is a high density of basic residues near the C-terminus (^{404}RRIQR^{408}). To our surprise, however, an antiparallel orientation is present in our structure, which is not consistent with the above model. There is an intermolecular electrostatic interaction between the basic residue Arg404 of the peptide and the acidic residue Glu84 of CaM which accounts for the antiparallel interaction.

3.3. Crystal structure of the Fas–CaM complex

In the Fas–CaM structure, although 25 residues covering helix 1 and helix 2 (^{230}SKYITTIAGVMTLSQVKGFVRK-NGV^{254}) of the death domain were synthesized and crystal-

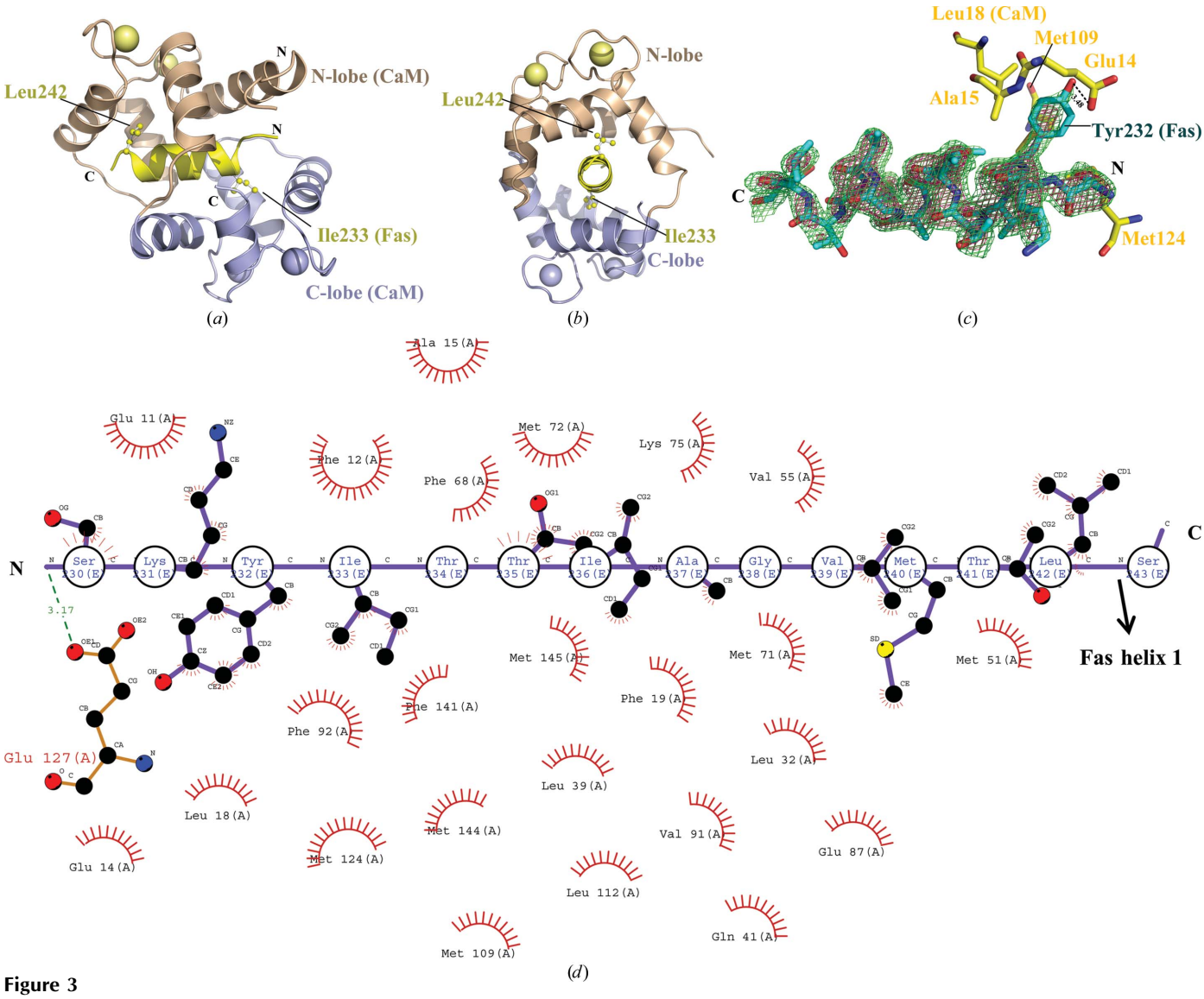

Figure 3
Crystal structure of the CaM–Fas complex. (*a*) Ribbon diagram of the complex. Wheat, CaM N-lobe; light blue, CaM C-lobe; yellow, Fas helix 1. Two key anchors (Ile233 and Leu242) are shown in ball-and-stick representation. (*b*) 90° rotation of (*a*). (*c*) A $2F_o - F_c$ peptide-omitted electron-density map (green, contoured at 1σ) and a $F_o - F_c$ map (red, contoured at 3σ) for Fas helix 1. Local interactions between CaM residues and Tyr232 are shown. Y232C is a naturally occurring single-point mutation in human ALPS. (*d*) *LIGPLOT* diagram detailing the interactions between CaM and Fas. The red eyelash shapes mark the CaM residues that make hydrophobic contacts with Fas helix 1.

lized, the C-terminal 11 residues (helix 2) are beyond the binding site and exhibit disordered electron density, and only the N-terminal 14 residues (helix 1; ^{230}SKYITTIAGVMTLS^{243}) can be well defined in the density map (Fig. 3*c*). The overall structure shows that CaM is a compact ellipsoidal structure containing a cavity which is occupied by the Fas peptide anchored in an antiparallel fashion (Figs. 3*a* and 3*b*). The peptide adopts an α-helical conformation and makes extensive contacts with CaM. The total buried surface area is about 2480 Å^2, of which approximately 61% is hydrophobic. It shows that the binding of Fas is largely driven by hydrophobic residues interacting with the hydrophobic surface cavities of CaM. It is worth noting that Tyr232 on Fas helix 1 is deeply buried within a hydrophobic pocket of CaM created by Ala15, Leu18, Met109 and Met124 (Fig. 3*c*). Importantly, Y232C is a naturally occurring single-point mutation associated with human autoimmune lymphoproliferative syndrome (ALPS; http://research.nhgri.nih.gov/ALPS/fas_tnfrsf6_exon9_mut.shtml).

Fas helix 1 engages two hydrophobic pockets of CaM lobes through two key anchors (Ile233 and Leu242) in a 1–10 motif, as in the CaM–CaMKII complex (Meador *et al.*, 1993) and as shown in Supplementary Fig. S3. Superposition of individual lobes with the CaM–smMLCK complex shows that the two anchors interact with CaM in a similar manner (Supplementary Fig. S4). However, the Fas peptide lacks a basic residue cluster, a feature common to most CaM-binding peptides, and therefore there is a lack of intermolecular electrostatic interactions (Fig. 3*d*). We speculate that if charge-coupling interactions cannot account for the binding orientation, the orientation may arise from the hydrophobic interactions, which form the vast majority of the CaM–target contacts.

3.4. Comparison of the p75^{NTR}–CaM complex and the Fas–CaM complex

An overlap of the two CaM structures shows no substantial changes in their C-lobe conformations, but significant changes were observed in the fourth helix of the N-lobes and in the linker between the two lobes (Figs. 4*a* and 4*b*). The root-mean-square deviation for the whole CaM structure is 0.95 Å. Arg405 of p75^{NTR} induces the fourth helix of CaM to make a conformational change from a normal three-turn helix to a two-turn helix. For both of the structures, the relative position of the two CaM lobes is more similar to that in complexes with inhibitors, such as trifluoperazine (Vandonselaar *et al.*, 1994) and KAR-2 (Horváth *et al.*, 2005), than with peptides. Both the p75^{NTR} and Fas peptides adopt the conformation of a three-turn helix of 11 or 12 residues in length surrounded by two loops. In contrast, most other CaM–peptide complexes assume a longer helical conformation (~4–6 turns). Intriguingly, there is a lack of significant similarity between p75^{NTR} and Fas regarding the positions and sequences of their CaM-binding sites. In contrast to the 1–10 binding motif in Fas, the two key anchors are spaced in a 1–11 motif in p75^{NTR}, which deviates from the classical CaM-target binding modes and thus represents a novel type of CaM recognition.

4. Discussion

Elucidation of the precise mechanisms behind the function of death receptors has been of longstanding interest. Although sharing a simple six-helix bundle structural feature, their death domains transduce a variety of biological effects. Apart from

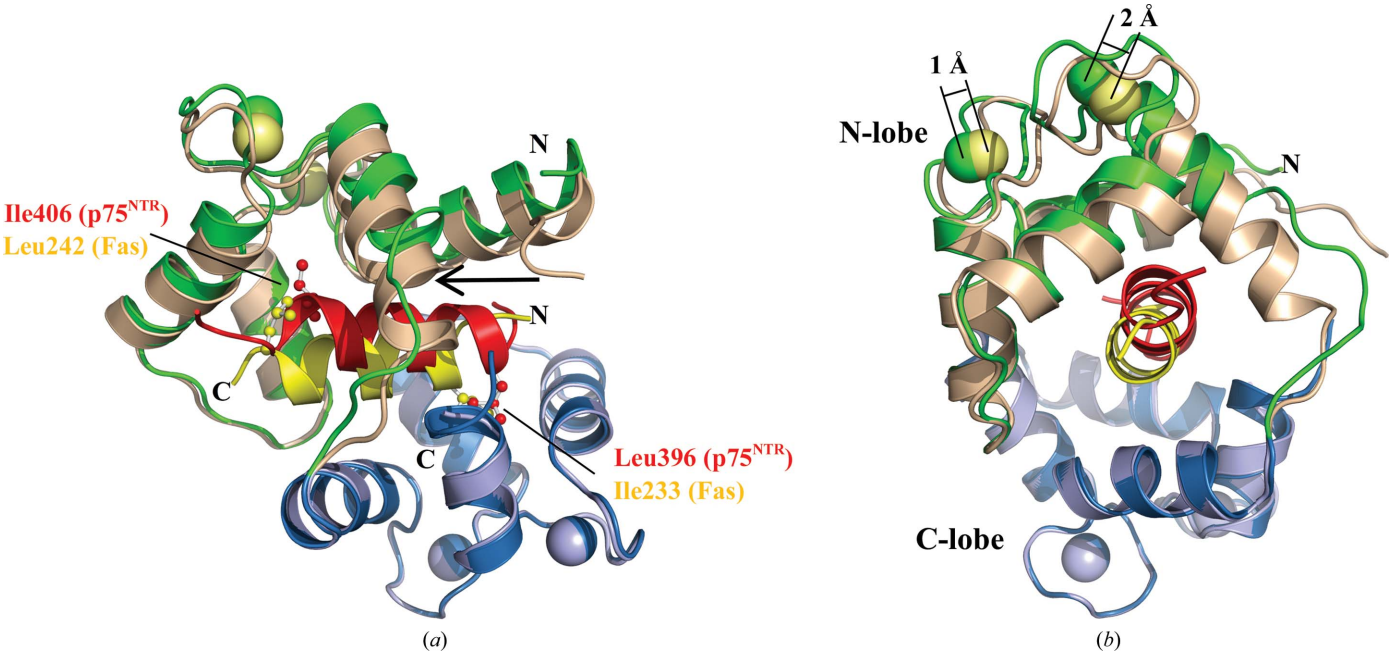

Figure 4
Comparisons between the CaM–Fas and CaM–p75^{NTR} complexes. (*a*) The CaM C-lobes were superimposed. The CaM N-lobe, the CaM C-lobe and helix 5 from the CaM–p75^{NTR} complex are shown in green, blue and red, respectively. The CaM N-lobe, the CaM C-lobe and helix 1 from the CaM–Fas complex are shown in wheat, light blue and yellow, respectively. Key anchors of peptides are labelled and shown in ball-and-stick respresentation. A significantly different region between the two structures is indicated by a black arrow. (*b*) 90° rotation of (*a*). The shifts in Ca^{2+} position are indicated.

apoptosis signals, they can convey other biological responses. For example, the prototypical death receptor Fas is normally engaged by FasL, resulting in the formation of DISC. In certain cell types, however, it conveys alternative non-apoptotic as well as proliferative signals involved in the control of inflammatory and immune responses (O'Reilly *et al.*, 2009). Intriguingly, both p75^{NTR} and DR6 can not only mediate neuronal apoptosis but can also affect cell survival in an anti-apoptotic manner (Benschop *et al.*, 2009; Nykjaer *et al.*, 2005). A chimeric receptor constructed from the extracellular portion of Fas and the intracellular portion of p75^{NTR} cannot induce apoptosis, whereas the expression of wild-type Fas readily induces cell death (Kong *et al.*, 1999). Thus, solving the structures of death receptors in complex with their downstream adaptor molecules should contribute greatly to the understanding of the signalling mechanisms involved. Our structural data provide molecular details of the interactions between the death domains and CaM. Their binding to CaM indicates that CaM is a common modulator of the death receptors Fas, p75^{NTR} and DR6. At the same time, two distinct CaM recognition sites and binding modes were revealed. These may contribute to the functional diversity of the death receptors.

4.1. The opening process of death domains during CaM binding

Models of the complexes of full-length Fas and p75^{NTR} with CaM were constructed using *PyMOL* based on the NMR

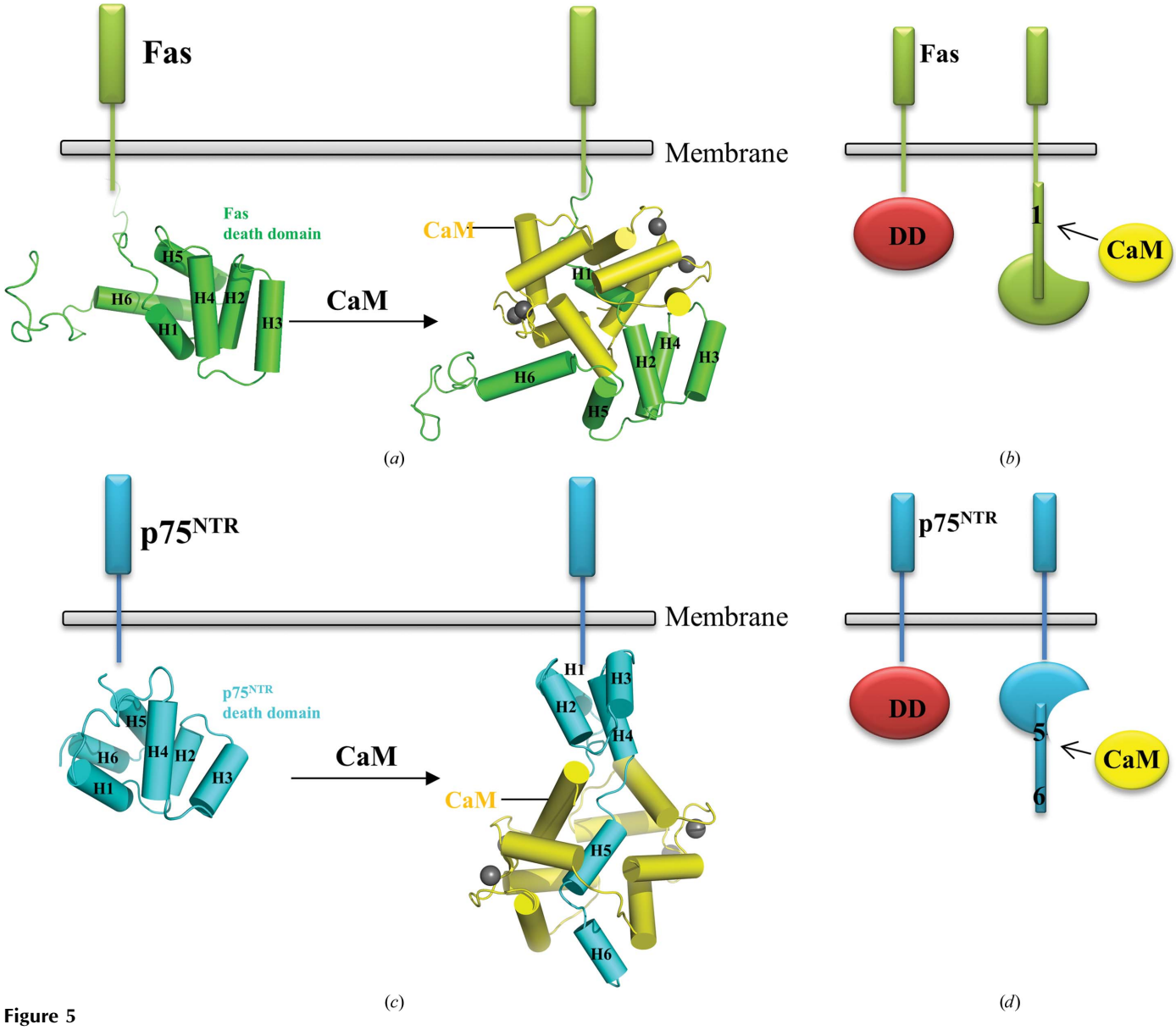

Figure 5
Models of CaM–full-length receptor complexes and a cartoon representation of the conformational changes. (*a*, *c*) Left: unbound death domains adapt a compact conformation according to the NMR structures (Huang *et al.*, 1996; Liepinsh *et al.*, 1997). Green, Fas death domain; blue, p75^{NTR} death domain. Right: models of the Fas/p75^{NTR}–CaM complex, presenting a noncompact conformation of the death domain upon binding of CaM (yellow). (*b*, *d*) In the cartoon representations, the native closed death domains (red) are shown on the left-hand side. Shown on the right are their opening modes. The numbers (H1–H6) indicate the helices of the death domains.

structures of death domains (Huang *et al.*, 1996; Liepinsh *et al.*, 1997) and our structures. In solution, the native conformations of both isolated death domains were shown to be a compact global fold. However, when in complex with CaM the death-domain conformation needs to deviate from the typical structure. For Fas, in order to make sufficient space for its CaM-grabbing helix 1, this helix needs to rotate by about 90° to stretch out, during which process it forms a nearly straight line with helix 2. In addition, the other helices may display less substantial changes moving away from helix 2 to avoid a steric clash with CaM (Fig. 5*a*). In order to expose its CaM-binding site, the $p75^{NTR}$ death domain also undergoes significant conformational changes (Fig. 5*c*). However, this occurs in a different fashion to Fas. Both helix 5 and helix 6 rotate by about 90° to form an almost straight line with helix 4, whereas the other helices show little change in their overall conformations. It appears that the opening process of death domains as discovered here would be a necessary event for CaM to bind to the death receptors.

4.2. Diverse opening modes and distinct recognition mechanisms

The two distinct opening states proposed in our models differ from the conformation of Fas in the high-resolution Fas–FADD complex described previously, in which helix 6 is stretched out and forms a long stem-helix with helix 5 in order to introduce both FADD binding and the pairing of two Fas receptors (Scott *et al.*, 2009). This implies that diverse signalling conformations of death domains may exist. We therefore propose a general mode of death-domain signalling (Figs. 5*b* and 5*d*). In the unbound death receptor, the six helices of the death domain are packed together in a compact manner. Upon binding CaM, the death domain may lose its compact structure and undergo conformational changes to an open state. Diverse opening modes may provide the base for recruiting appropriate partners such as CaM, FADD or TRADD *etc.* It is noteworthy that another mechanism without the opening process (Ferrao & Wu, 2012; Wang *et al.*, 2010) may also exist, and it remains a challenge for future investigations to identify the underlying structural and functional details.

4.3. The functional role of CaM for the death receptors

Changes in the cytosolic Ca^{2+} concentration are highly regulated in order to control diverse biological processes (Hoeflich & Ikura, 2002). Here, we found that the interaction between the death receptors and CaM is Ca^{2+}-dependent, indicating that alteration of their binding will be affected by local changes in the intracellular Ca^{2+} concentration.

Previous studies showed that CaM is associated with Fas-mediated apoptosis (Ahn *et al.*, 2004; Chen *et al.*, 2008) and that helix 1 of the Fas death domain (*i.e.* the CaM-binding site as reported here) plays an important role in interacting with FADD directly (Scott *et al.*, 2009). This suggests that the CaM–Fas interaction would modulate FADD binding in apoptosis. Coincidently, helix 5 of $p75^{NTR}$ (*i.e.* the CaM-binding site as reported here) is identical to the region that is sufficient on its own to induce $p75^{NTR}$-mediated apoptosis, and Arg404 and Arg405 appear to play a key role within this helix. Mutations of these residues to Glu resulted in the loss of this pro-apoptotic effect (Rabizadeh *et al.*, 2000). In addition, helix 5 of $p75^{NTR}$ is identical to the region necessary for interaction with Rho-GDI, the Rho GDP-dissociation inhibitor (Yamashita & Tohyama, 2003). Thus, it appears that there is potential competition for the same binding site between downstream partners and CaM, which implies a special mechanism for the death receptors from the upstream Ca^{2+} signal to downstream events.

Our findings help to expand the spectrum of CaM-binding targets and their functional roles. It will facilitate our understanding of the role that CaM plays in regulating the signal transduction pathways elicited by the death receptors Fas, $p75^{NTR}$ and DR6. A potential relationship between CaM and the death domains has been proposed, upon which further experimental investigation both *in vivo* and *in vitro* will be undertaken. Naturally, it is still possible that the interactions may be related to the intracellular cross-talk signalling pathways, because CaM can bind a diverse array of other cellular molecules. Furthermore, the peptides $p75^{NTR}$ helix 5, Fas helix 1 and DR6 helix 5 can be used as inhibitors of CaM association with the corresponding death receptors, which may allow the design of peptide agents for potential therapeutic applications in Fas-induced autoimmune disease or $p75^{NTR}$/DR6-induced neurodegenerative disease.

We thank Yuanyuan Chen for performing the SPR assay, Yi Han and Shengquan Liu for X-ray diffraction data collection and Hongjun Yu for CaM expression. We are grateful to Deyu Zhu and Yuanyuan Chen for critical reading of the manuscript. This research was financially supported by grants from the National Natural Science Foundation of China (Grant Nos. 30970567, 31025009, 31270791 and 31021062), the Knowledge Innovation Program of the Chinese Academy of Sciences (Grant No. KSCX2-EW-Q-11) and the Ministry of Science and Technology (973 Program, Grant No. 2012CB911100).

References

Ahn, E.-Y., Lim, S.-T., Cook, W. J. & McDonald, J. M. (2004). *J. Biol. Chem.* **279**, 5661–5666.
Benschop, R., Wei, T. & Na, S. (2009). *Therapeutic Targets of the TNF Superfamily*, edited by I. S. Grewal, pp. 186–194. New York: Springer.
Brünger, A. T., Adams, P. D., Clore, G. M., DeLano, W. L., Gros, P., Grosse-Kunstleve, R. W., Jiang, J.-S., Kuszewski, J., Nilges, M., Pannu, N. S., Read, R. J., Rice, L. M., Simonson, T. & Warren, G. L. (1998). *Acta Cryst.* D**54**, 905–921.
Chen, Y., Pawar, P., Pan, G., Ma, L., Liu, H. & McDonald, J. M. (2008). *J. Cell. Biochem.* **103**, 788–799.
Egea, J., Espinet, C., Soler, R. M., Dolcet, X., Yuste, V. J., Encinas, M., Iglesias, M., Rocamora, N. & Comella, J. X. (2001). *J. Cell Biol.* **154**, 585–597.
Egea, J., Espinet, C., Soler, R. M., Peiró, S., Rocamora, N. & Comella, J. X. (2000). *Mol. Cell. Biol.* **20**, 1931–1946.
Emsley, P. & Cowtan, K. (2004). *Acta Cryst.* D**60**, 2126–2132.
Ferrao, R. & Wu, H. (2012). *Curr. Opin. Struct. Biol.* **22**, 241–247.

Gong, Y., Cao, P., Yu, H.-J. & Jiang, T. (2008). *Nature (London)*, **454**, 789–793.
Gouet, P., Courcelle, E., Stuart, D. I. & Métoz, F. (1999). *Bioinformatics*, **15**, 305–308.
Hoeflich, K. P. & Ikura, M. (2002). *Cell*, **108**, 739–742.
Hong, K., Nishiyama, M., Henley, J., Tessier-Lavigne, M. & Poo, M. (2000). *Nature (London)*, **403**, 93–98.
Horváth, I., Harmat, V., Perczel, A., Pálfi, V., Nyitray, L., Nagy, A., Hlavanda, E., Náray-Szabó, G. & Ovádi, J. (2005). *J. Biol. Chem.* **280**, 8266–8274.
Huang, B., Eberstadt, M., Olejniczak, E. T., Meadows, R. P. & Fesik, S. W. (1996). *Nature (London)*, **384**, 638–641.
Ibáñez, C. F. & Simi, A. (2012). *Trends Neurosci.* **35**, 431–440.
Kincaid, R. L., Billingsley, M. L. & Vaughan, M. (1988). *Methods Enzymol.* **159**, 605–626.
Kong, H., Kim, A. H., Orlinick, J. R. & Chao, M. V. (1999). *Cell Death Differ.* **6**, 1133–1142.
Laskowski, R. A., MacArthur, M. W., Moss, D. S. & Thornton, J. M. (1993). *J. Appl. Cryst.* **26**, 283–291.
Lavrik, I., Golks, A. & Krammer, P. H. (2005). *J. Cell Sci.* **118**, 265–267.
Li, Y., Jia, Y.-C., Cui, K., Li, N., Zheng, Z.-Y., Wang, Y.-Z. & Yuan, X.-B. (2005). *Nature (London)*, **434**, 894–898.
Liepinsh, E., Ilag, L. L., Otting, G. & Ibáñez, C. F. (1997). *EMBO J.* **16**, 4999–5005.
Matsubara, M., Nakatsu, T., Kato, H. & Taniguchi, H. (2004). *EMBO J.* **23**, 712–718.
Maximciuc, A. A., Putkey, J. A., Shamoo, Y. & Mackenzie, K. R. (2006). *Structure*, **14**, 1547–1556.
Mc Guire, C., Beyaert, R. & van Loo, G. (2011). *Trends Neurosci.* **34**, 619–628.
Meador, W. E., Means, A. R. & Quiocho, F. A. (1992). *Science*, **257**, 1251–1255.
Meador, W. E., Means, A. R. & Quiocho, F. A. (1993). *Science*, **262**, 1718–1721.
Murshudov, G. N., Skubák, P., Lebedev, A. A., Pannu, N. S., Steiner, R. A., Nicholls, R. A., Winn, M. D., Long, F. & Vagin, A. A. (2011). *Acta Cryst.* D**67**, 355–367.
Nykjaer, A., Willnow, T. E. & Petersen, C. M. (2005). *Curr. Opin. Neurobiol.* **15**, 49–57.
O' Reilly, L. A., Tai, L., Lee, L., Kruse, E. A., Grabow, S., Fairlie, W. D., Haynes, N. M., Tarlinton, D. M., Zhang, J. G., Belz, G. T., Smyth, M. J., Bouillet, P., Robb, L. & Strasser, A. (2009). *Nature (London)*, **461**, 659–663.
Osawa, M., Tokumitsu, H., Swindells, M. B., Kurihara, H., Orita, M., Shibanuma, T., Furuya, T. & Ikura, M. (1999). *Nature Struct. Biol.* **6**, 819–824.
Otwinowski, Z. & Minor, W. (1997). *Methods Enzymol.* **276**, 307–326.
Pan, D., Yan, Q., Chen, Y., McDonald, J. M. & Song, Y. (2011). *Proteins*, **79**, 2543–2556.
Park, H. H., Lo, Y.-C., Lin, S.-C., Wang, L., Yang, J. K. & Wu, H. (2007). *Annu. Rev. Immunol.* **25**, 561–586.
Rabizadeh, S. *et al.* (2000). *J. Mol. Neurosci.* **15**, 215–229.
Salvesen, G. S. & Riedl, S. J. (2009). *Cell Cycle*, **8**, 2723–2727.
Scott, F. L., Stec, B., Pop, C., Dobaczewska, M. K., Lee, J. J., Monosov, E., Robinson, H., Salvesen, G. S., Schwarzenbacher, R. & Riedl, S. J. (2009). *Nature (London)*, **457**, 1019–1022.
Vagin, A. & Teplyakov, A. (2010). *Acta Cryst.* D**66**, 22–25.
Vandonselaar, M., Hickie, R. A., Quail, J. W. & Delbaere, L. T. J. (1994). *Nature Struct. Biol.* **1**, 795–801.
Vetter, S. W. & Leclerc, E. (2003). *Eur. J. Biochem.* **270**, 404–414.
Wallace, A. C., Laskowski, R. A. & Thornton, J. M. (1995). *Protein Eng.* **8**, 127–134.
Wang, L., Yang, J. K., Kabaleeswaran, V., Rice, A. J., Cruz, A. C., Park, A. Y., Yin, Q., Damko, E., Jang, S. B., Raunser, S., Robinson, C. V., Siegel, R. M., Walz, T. & Wu, H. (2010). *Nature Struct. Mol. Biol.* **17**, 1324–1329.
Wilson, N. S., Dixit, V. & Ashkenazi, A. (2009). *Nature Immunol.* **10**, 348–355.
Winn, M. D. *et al.* (2011). *Acta Cryst.* D**67**, 235–242.
Wu, X., Ahn, E. Y., McKenna, M. A., Yeo, H. & McDonald, J. M. (2005). *J. Biol. Chem.* **280**, 29964–29970.
Yamashita, T. & Tohyama, M. (2003). *Nature Neurosci.* **6**, 461–467.